The Astrophysical Journal Letters, 844:L18 (6pp), 2017 August 1 https://doi.org/10.3847/2041-8213/aa7851

Carbon Chain Anions and the Growth of Complex Organic Molecules in Titan's Ionosphere

R. T. Desai[1,2], A. J. Coates[1,2], A. Wellbrock[1,2,9], V. Vuitton[3], F. J. Crary[4], D. González-Caniulef[1], O. Shebanits[5,6], G. H. Jones[1,2], G. R. Lewis[1], J. H. Waite[7], M. Cordiner[8], S. A. Taylor[1,2], D. O. Kataria[1], J.-E. Wahlund[5,6], N. J. T. Edberg[6], and E. C. Sittler[8]
[1] Mullard Space Science Laboratory, University College London, Holmbury St. Mary, Surrey RH5 6NT, UK; r.t.desai@ucl.ac.uk
[2] Centre for Planetary Science at UCL/Birkbeck, London, Gower Street, London WC1E 6BT, UK
[3] Université Grenoble Alpes, CNRS, IPAG, F-38000 Grenoble, France
[4] Laboratory for Atmospheric and Space Physics, University of Colorado, Innovation Drive, Boulder, CO 80303, USA
[5] Department of Physics and Astronomy, Uppsala University, Box 516, SE-751 20 Uppsala, Sweden
[6] Swedish Institute of Space Physics, Box 537, SE-751 21 Uppsala, Sweden
[7] Space Science and Engineering Division, Southwest Research Institute (SWRI), 6220 Culebra Road, San Antonio, TX 78238, USA
[8] NASA Goddard Space Flight Center, 8800 Greenbelt Road, Greenbelt, MD 20771, USA
Received 2017 April 16; revised 2017 May 27; accepted 2017 June 1; published 2017 July 26

Abstract

Cassini discovered a plethora of neutral and ionized molecules in Titan's ionosphere including, surprisingly, anions and negatively charged molecules extending up to 13,800 u q^{-1}. In this Letter, we forward model the *Cassini* electron spectrometer response function to this unexpected ionospheric component to achieve an increased mass resolving capability for negatively charged species observed at Titan altitudes of 950–1300 km. We report on detections consistently centered between 25.8 and 26.0 u q^{-1} and between 49.0–50.1 u q^{-1} which are identified as belonging to the carbon chain anions, CN^-/C_3N^- and/or C_2H^-/C_4H^-, in agreement with chemical model predictions. At higher ionospheric altitudes, detections at 73–74 u q^{-1} could be attributed to the further carbon chain anions C_5N^-/C_6H^- but at lower altitudes and during further encounters extend over a higher mass/charge range. This, as well as further intermediary anions detected at >100 u, provide the first evidence for efficient anion chemistry in space involving structures other than linear chains. Furthermore, at altitudes below <1100 km, the low-mass anions (<150 u q^{-1}) were found to deplete at a rate proportional to the growth of the larger molecules, a correlation that indicates the anions are tightly coupled to the growth process. This study adds Titan to an increasing list of astrophysical environments where chain anions have been observed and shows that anion chemistry plays a role in the formation of complex organics within a planetary atmosphere as well as in the interstellar medium.

Key words: astrobiology – astrochemistry – ISM: molecules – planets and satellites: atmospheres – planets and satellites: individual (Titan)

1. Introduction

Titan is the second largest moon in the solar system (radius $R_T = 2576$ km) and possesses a dense extended atmosphere principally composed of ~96% molecular nitrogen, <4% methane, and <1% hydrogen (Vervack et al. 2004; Niemann et al. 2005; Waite et al. 2005). Aerosol-type particles envelop the moon in a thick organic photochemical haze (Danielson et al. 1973), a phenomenon also present at Pluto (Gladstone et al. 2016), Triton (Broadfoot et al. 1989), the Archean Earth (Miller & Urey 1959), and likely also methane-rich extra-solar planets. The production mechanisms and composition of these naturally occurring organic compounds are, however, far from understood.

The *Cassini* spacecraft has sampled the ionized regions of Titan's upper atmosphere down to altitudes of <900 km in situ and observed positively charged ions (cations) extending up to nearly 1000 u q^{-1}(Crary et al. 2009; Coates et al. 2010) and, surprisingly, negatively charged ions (anions) and aerosol precursors extending up to 13,800 u q^{-1} (Coates et al. 2007, 2009; Waite et al. 2007). The cations were detected at nearly all masses up to 100 u with over 50 species identified in this range (Cravens et al. 2006; Vuitton et al. 2007). At >100 u, evidence for carbon-based aromatic compounds has been reported, although unique identifications were not possible (Crary et al. 2009; Wahlund et al. 2009; Westlake et al. 2014). The anions and larger negatively charged molecules were obtained at a lower resolution and classified into broad mass groupings of 12–30, 30–55, 55–90, 90–125, 125–195, 195–625, and 625+ u q^{-1} with the higher masses observed at lower altitudes and higher latitudes (Coates et al. 2007; Wellbrock et al. 2013). In the deep ionosphere below ~1000 km, the anion/aerosol precursor charge density was observed to exceed that of the electrons resulting in an ion–ion (dusty) plasma (Shebanits et al. 2013, 2016).

A number of studies have modeled the cation and neutral chemistry occurring in Titan's ionosphere at <100 u q^{-1}, but only two studies have attempted to model the anion chemistry (Vuitton et al. 2009a; Dobrijevic et al. 2016). These focused on low-mass species of <75 u and in particular inferred the presence of the $C_{n-1}N^-$ and C_nH^- anions, where $n = 2$–6. These carbon chain anions have all also been detected in dark molecular clouds, prestellar cores, or protostellar envelopes (Cordiner et al. 2013; Millar et al. 2017) where their high reactivity acts as a catalyst for the formation of larger organic molecules (Millar et al. 2000; Walsh et al. 2009). Chemical

[9] Creator of AASTeX v6.1.

models of these environments also predict even larger anions containing up to 23 carbon atoms (Bettens & Herbst 1996).

At Titan, chemical schemes are only beginning to provide theories as to how the larger species can be produced. Stochastic charging models provide some explanation for how species of ~100 u could be ionized and aggregate to form >10,000 u molecules (Michael et al. 2011; Lavvas et al. 2013; Lindgren et al. 2016), but only a few studies have looked at precise chemical routes for producing molecules >100 u. Westlake et al. (2014) demonstrate how cations of >100 u are likely formed from smaller hydrocarbon compounds through ion–molecule growth processes, and Ali et al. (2015) provided a mechanistic analysis of possible routes from small to large cations of <250 u q^{-1}. The latter was based upon Olah's three-membered Hückel aromatic rings (Olah 1972; Olah et al. 2016) and suggests the presence of several carbocations and their corresponding carbanions.

This Letter provides analysis of the anion and aerosol precursor data set using a forward model of the *Cassini* Plasma Spectrometer (CAPS) Electron Spectrometer (ELS) instrument response function to these species. Statistical evidence for the low-mass carbon chain anions, CN^-/C_2H^- and C_3N^-/C_4H^-, is presented, as well as constraints on intermediary anions in the range of 50–200 u q−1. The role of these species is then examined with respect to the growth of larger molecules with decreasing altitude.

2. Methodology

The results presented in this Letter are derived from CAPS-ELS observations obtained during the T16, T18, T32, T40, and T48 encounters. These include measurements across Titan's sunlit (T16 ingress, T18, T32 ingress, T40, T48) and anti-sunlit (T16 egress and T32 egress) hemispheres, a variety of latitudes, and also when Titan was immersed directly within the solar wind (T32). Further information on the geometry and ambient conditions of the Titan encounters can be found in Coates et al. (2009).

The CAPS-ELS is a top-hat electrostatic-analyzer sensitive to negatively charged particles in the 0.6–28,000 eV range (Young et al. 2004). Anions can be identified within the ELS three-dimensional velocity distribution due to being highly supersonic in the spacecraft frame and preferentially registering in anodes aligned with the spacecraft velocity vector. Thus, as *Cassini* travels through Titan's ionosphere, the ELS observes an anion mass/charge spectrum

$$\frac{m}{q} = \frac{2}{q v_{\rm sc}^2}(E_{\rm ELS} - \phi_{\rm sc}), \tag{1}$$

where $E_{\rm ELS}$ is the nominal acceptance energy, $v_{\rm sc}$ is the spacecraft velocity relative to Titan, and $\phi_{\rm sc}$ is the ELS spacecraft potential shift applied in accordance with Liouville's theorem (Lewis et al. 2008). To isolate the anion detections, the count rates are taken from each scan across the ram direction and the isotropically observed electrons on non-ram-pointing anodes are averaged and subtracted. The count rate R_C, can then be related to the number density, $n_{\rm ni}$, using the ion current approximation (Coates et al. 2007; Waite et al. 2007):

$$n_{\rm ni} = \frac{R_c}{v_{\rm sc} A_F \varepsilon}, \tag{2}$$

where $A_F = 0.33$ cm^2 is the effective area of acceptance, and ε is the Microchannel Plate anion detection efficiency function that is energy dependent. A value of $\varepsilon = 0.05$ was used in previous studies based upon the extensive study by Fraser (2002), which remains the best estimate for the larger species. Studies have, however, shown that at lower energies this could be significantly larger for negatively charged molecules (e.g., Peko & Stephen 2010) where electron multiplication is increasingly dependent on potential as well as kinetic emission processes (Hagstrum 1976). Further analysis of the density uncertainties will be addressed by A. Wellbrock et al. (in preparation), and in this study we do not implement a new value.

The ELS energy bins are quasi-logarithmically spaced to match the energy resolution and overlap at FWHM. This results in a nominal electron or anion distribution registering counts across multiple energy bins. To take this into account, we forward model the ELS response to anions. The ELS $\Delta E/E$ resolution can be represented using a normalized Gaussian of the form

$$f(E) = R_{\rm nc} \exp\left(-\frac{1}{2}\left(\frac{E - E_0}{E_W}\right)^2\right), \tag{3}$$

where E_0 is the center of the distribution, E_W is the width, and $R_{\rm nc}$ is the normalized count rate. Here, E_W corresponds to $\Delta E/E = 16.7\%$ in the case of a single anion distribution but can be larger in the case of multiple overlapping distributions. The thermal energy spread of the anions is approximated by a drifting Maxwellian expressed in count rates:

$$g(E) = \frac{2nE^2G}{\sqrt{m}}\left(\frac{1}{2\pi kT}\right)^{\frac{3}{2}} \exp\left(-\frac{(E - E_0)}{kT}\right), \tag{4}$$

as adapted from Rymer et al. (2001), where T is the ion temperature in Titan's ionosphere and G the geometric factor

$$G = A_F \frac{\Delta E}{E}\varepsilon, \tag{5}$$

which is derived under the assumption that the anion current fills the ELS aperture. The ion temperature in Titan's ionosphere has been determined to be significantly less than the $\Delta E/E$ instrument sensitivity, and tests with or without this thermal contribution produced similar results. In this study, it is therefore held constant at at $kT = 0.02$ eV (Crary et al. 2009) and included for completeness. The ELS response function and the anion distribution can then be convolved,

$$h(E) = f(E) * g(E), \tag{6}$$

and the resulting function modeled to fit the observed data using a χ^2 minimization routine.

Of further note is that the spacecraft surfaces charge to negative values in Titan's relatively dense ionosphere, and the various surfaces will also charge to different potentials based upon variations in material conductivities and incident electron and ion currents (Crary et al. 2009). This results in the exact potential correction, $\phi_{\rm sc}$, also being unknown, and the centers of the fitted distributions are therefore established relative to one another.

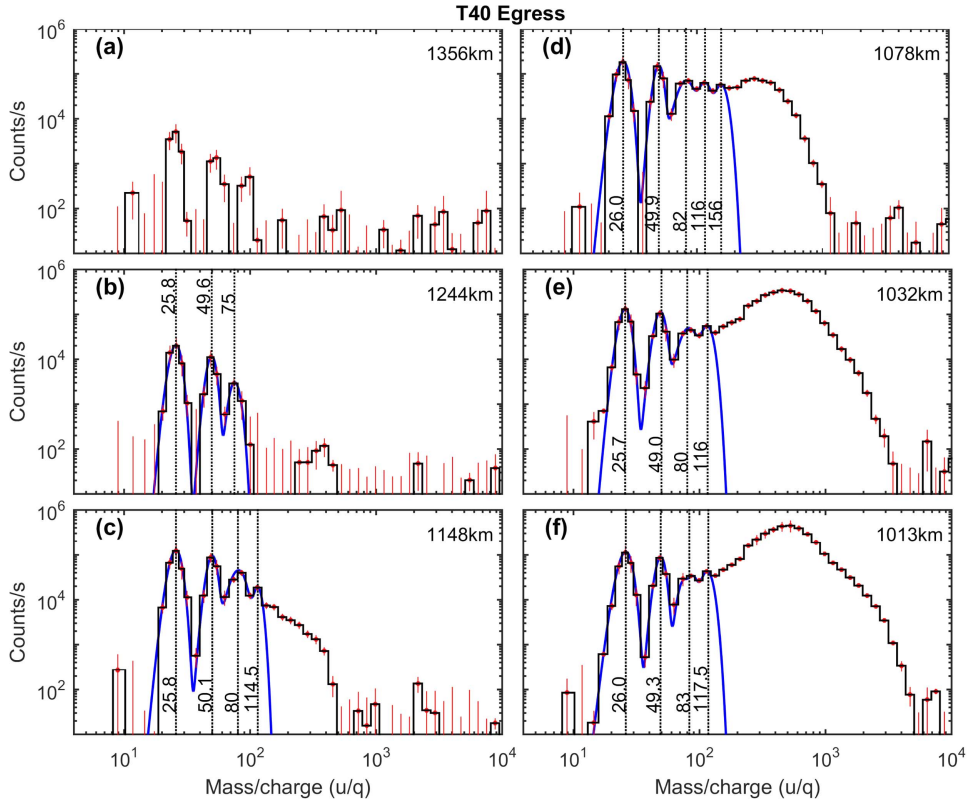

Figure 1. Histogram of the CAPS-ELS anion mass/charge spectrum at various altitudes within Titan's ionosphere during the T40 encounter. The fitting routine (blue) and error bars (red) are calculated as described in Equations (1)–(7). The nominal center of each group is marked (dotted black line), and the fitting parameters are given in Table 1.

Errors in the observed count rates are taken as

$$\sigma = \sigma_p + \sigma_{\rm std}, \tag{7}$$

where σ_p corresponds to the Poisson counting statistics and $\sigma_{\rm std}$ corresponds to the standard deviation of counts on non-ram-oriented anodes. This is used as a measure of electron anisotropies and inter-anode scaling uncertainties, introduced when isolating the anion detections.

3. Species Identification

Figure 1 shows the anion mass/charge spectrum measured at various altitudes during T40. At higher altitudes (>1300 km) the larger >100 u q^{-1} species are absent, and at the highest altitudes it is difficult to identify anions due to decreased densities. As *Cassini* descends, clear detections appear at <200 u q^{-1} and the larger >200 u q^{-1} distribution starts to grow below ~1250 km. The five resolved clustered detections in the spectra are hereafter referred to as peaks 1–5 and fall within the range of mass groups 1–5 as described by Wellbrock et al. (2013). Figure 2 also shows anion spectra obtained during encounters T16, T18, T32, and T48.

The fitting procedure applied to peaks 1 and 2 finds the center of the primary two peaks to be separated by 23–24.3 u q^{-1} in all encounters; see Table 1. Chemical models for Titans atmosphere predict efficient production of C_nH^- and $C_{n-1}N^-$ to result from dissociative electron attachment to, or de-protonation of, parent neutral species C_nH_2 and $HC_{n-1}N$ (Vuitton et al. 2009a; Dobrijevic et al. 2016). For example, CN^- and C_3N^- are produced by

$$HCN + e^- \rightarrow H + CN^-, \tag{8}$$

$$HC_3N + CN^- \rightarrow HCN + C_3N^-, \tag{9}$$

which proceeds rapidly due to abundant HCN and HC_3N. A similar reaction sequence exists for hydrocarbons where C_2H^- and C_4H^- are produced by

$$C_2H_2 + e^- \rightarrow H + C_2H^-, \tag{10}$$

$$C_4H_2 + C_2H^- \rightarrow C_2H_2 + C_4H^-. \tag{11}$$

due to abundance C_2H_2 and C_4H_2. This 23–24.3 u q^{-1} separation in the ELS mass/charge spectrum is indicative of these processes and the CN^-/C_2H^- and C_3N^-/C_4H^- carbon chain anions as the dominant constituents within the primary and secondary peaks, respectively. It is not possible to further resolve the 1 u difference between these nitrile and hydrocarbon compounds, but CN^- is estimated to be two orders of magnitude more abundant than C_2H^-, and C_3N^- and C_4H^- are predicted in comparable abundances (Vuitton et al. 2009a). The main anion loss process considered is associative detachment with neutral radicals.

The width of the primary peak is, however, often larger than the ELS $\Delta E/E \approx 16.7\%$. This can be explained by a multispecies composition, with further possible anion species such as C_2^-, $CH^-_{1,2,3}$, $NH^-_{1,2,3}$, and CO^- possibly contributing, the latter due to the introduction of water-group ions (O^+, OH^+, H_2O^+, H_3O^+) from Enceladus (Hartle et al. 2006; Cravens et al. 2008). It is, however, possible that the spacecraft potential also acts to spread a given distribution's energy

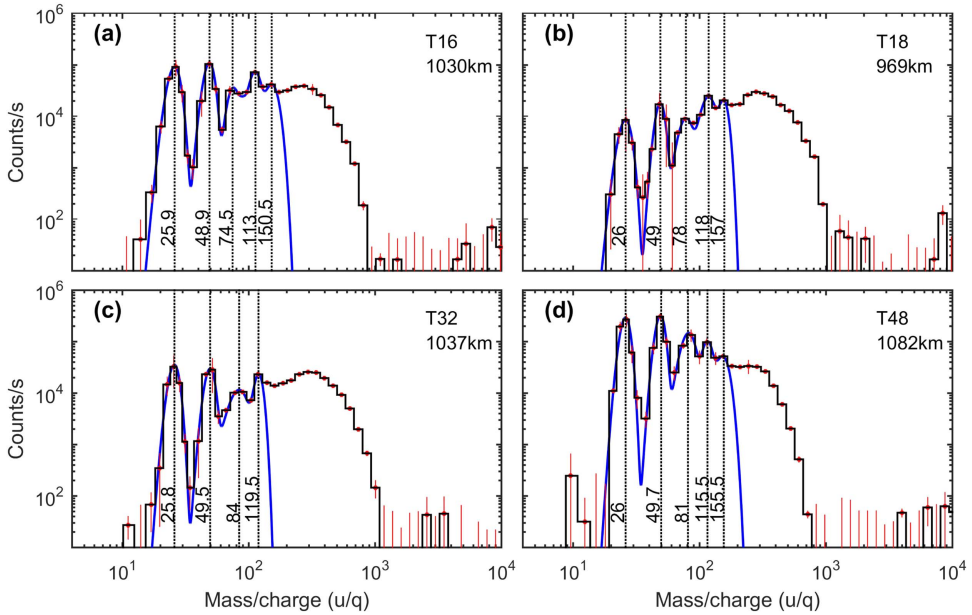

Figure 2. Histogram of the CAPS-ELS anion mass/charge spectrum during the T16, T18, T32, and T48 encounters. The fitting routine (blue) and error bars (red) are calculated as described in Equations (1)–(11). The nominal center of each group is marked (dotted black line), and the fitting parameters provided in Table 1.

relative to the spacecraft, an effect that would be more pronounced for lower-mass ions due to their lower inertia. The width of the secondary C_3N^-/C_4H^- peak falls across a range that encompasses the FWHM of the ELS, indicating this is likely composed of a single distribution function with only a minor contribution from further species possible.

This analysis indicates the spacecraft potential experienced by the ELS is 0.4–0.9 V more negative than that measured by the Radio and Plasma Wave Science (RPWS) Langmuir Probe (LP), although it is within the −3.5 V absolute range observed by the instrument in Titan's ionosphere (Crary et al. 2009). An ∼−0.3 V discrepancy was found between conjugate CAPS Ion Beam Spectrometer (IBS) and *Cassini*'s Ion and Neutral Mass Spectrometer (INMS) observations (Crary et al. 2009), and a more negative spacecraft potential correction is expected for anion detections (Jones et al. 2011). This is due to focusing effects where the spacecraft-generated potential field acts to deflect incident ions such that the anions arrive from a direction closer to the spacecraft surface.

At 1244 km (Figure 1(b)) the third peak is also visible where at higher altitudes it appears compatible with C_5N^-/C_6H^-; although this cannot be statistically verified as at >50 u q^{-1}, there are fewer measurements than free parameters. At lower altitudes this peak widens, extending as high as ∼94 u q^{-1} in some instances. This range does not include any previously observed anions and indicates the presence of anionic structures other than linear chains. INMS and CAPS-IBS measurements at these altitudes also show a grouping of neutrals and cations over a similar range (Waite et al. 2007; Crary et al. 2009), the most abundant of which was inferred to be benzene (C_6H_6; Vuitton et al. 2008). This is particularly relevant as benzene and benzene products are thought to be the seeds for larger aromatic compounds (Vuitton et al. 2009b). The lack of reaction rates and known chemical pathways at these high masses severely restricts the analysis of the anion chemistry, but several candidate species can be suggested. For example, the cyclic radical $C_6H_5^+$ is observed in appreciable quantities (Vuitton et al. 2009b) and can be a source for $C_6H_5^-$ anion radical production (Fenzlaff & Illenberger 1984). The stable $C_6H_7^-$ cyclic anion can also be produced through the interaction of benzene with H^- (Coletti & Nazzareno 2012). H^- cannot be measured, however, due to constraints imposed by the spacecraft velocity (see Equation (1)), but H^- fluxes can result from the interaction of methane with ionospheric electrons (Dobrijevic et al. 2016).

The four further encounters in Figure 2 also show this third peak to be the most variable between encounters, possibly indicating an enhanced sensitivity to the ambient conditions. A number of azine anions resulting from benzene, pyridine, pyridazine, pyrazine, and s-triazine have been explored by Wang et al. (2015) with application to Titan and determined to be highly reactive with nitrogen and oxygen. These include $C_6H_3^-$, $C_5H_2N^-$, $C_5H_3N^-$, $C_5H_4N^-$, $C_4H_3N_2^-$, and $C_3H_2N_3^-$ and are of high astrobiological interest. The higher end of this third mass range is, however, less explored, and further anions such as the benzyl anion $C_7H_7^-$ and anilinide anion $C_6NH_6^-$ (Wang & Biermaum 2016) could be derived from the >20 mostly polyaromatic hydrocarbons and nitrated heterocyclic species suggested in this range.

At altitudes <1200 km a fourth distinct peak, with consistent detections at ∼117 ± 3 u q^{-1}, is identified during every encounter. This appears at count rates comparable to the primary peaks and sometimes double that of the neighboring peaks. This is most evident during T16 where the highest-mass species at 13,800 u q^{-1} were observed (Coates et al. 2009). A smaller fifth peak, with detections consistently at ∼154 ± 8 u q^{-1}, is also sometimes present. The >100 u q^{-1} regime is, however, even more unconstrained. It should be noted though that Trainer et al. (2013) detected ring structures near 117 u in laboratory simulations of aerosol-tholin production, which could represent growth processes involving aromatic rings at Titan.

Multiply charged anionic states are not considered here due to inter-electron repulsive forces making this phenomena increasingly unlikely for smaller molecules. This is evident as the smallest known multiply charged anions, C_n^{2-} (n = 7–28), have lifetimes of tens of microseconds in the gas

Table 1
Fitting Results for Peaks 1–5 in the CAPS-ELS Anion Mass/Charge Spectrum at <200 u q^{-1} as Marked in Figures 1 and 2

Flyby	Alt.	$\tilde{\chi}^2$	Peak 1		Peak 2		Peak 3	Peak 4	Peak 5	Potential (ϕ_{sc})	
			Center	FWHM	Center	FWHM	Range	Range	Range	RPWS-LP	ELS
(#)	(km)	(−)	(u q^{-1})	(%)	(u q^{-1})	(%)	(u q^{-1})	(u q^{-1})	(u q^{-1})	(V)	(V)
T40	1244	→0	$25.8^{+0.8}_{-0.6}$	$20.1^{+2.6}_{-4.6}$	$49.6^{+1.8}_{-1.5}$	20.9+	72–78	⋯	⋯	−0.63	−1.05
⋯	1148	1.50	$25.8^{+0.9}_{-0.5}$	$21.7^{+2.1}_{-3.3}$	$50.1^{+1.1}_{-0.8}$	$17.9^{+1.5}_{-2.7}$	71–89	109–120	⋯	−0.59	−1.20
⋯	1078	0.67	$26.0^{+0.4}_{-0.6}$	$21.6^{+0.6}_{-2.8}$	$49.9^{+2.0}_{-1.1}$	$17.0^{+2.2}_{-3.5}$	73–91	108–122	146–166	−0.58	−1.20
⋯	1032	0.72	$25.7^{+0.5}_{-0.5}$	$22.7^{+0.6}_{-2.0}$	$49.0^{+0.8}_{-0.5}$	$19.6^{+1.4}_{-2.0}$	73–91	109–123	⋯	−0.57	−1.20
⋯	1013	2.46	$26.0^{+0.8}_{-0.6}$	$22.7^{+1.9}_{-2.9}$	$49.3^{+0.6}_{-0.6}$	$18.1^{+1.0}_{-1.6}$	72–94	107–128	⋯	−0.59	−1.20
T16	1031	0.88	$25.9^{+0.4}_{-0.6}$	$22.8^{+2.5}_{-6.0}$	$48.9^{+0.7}_{-0.7}$	$19.6^{+1.6}_{-2.2}$	72–77	108–118	141–160	−0.66	−1.40
T18	969	0.73	$26.0^{+0.9}_{-1.0}$	$22.8^{+3.7}_{-6.2}$	$49.0^{+1.5}_{-0.7}$	$17.0^{+2.0}_{-2.1}$	74–82	113–123	148–166	−1.65	−2.50
T32	1036	0.92	$25.8^{+0.6}_{-1.1}$	$18.5^{+3.7}_{-2.4}$	$49.5^{+0.8}_{-1.2}$	$18.5^{+1.8}_{-3.5}$	74–94	114–125	⋯	−0.80	−1.55
T48	1082	2.18	$26.0^{+0.2}_{-0.2}$	$18.3^{+0.7}_{-0.4}$	$49.7^{+0.7}_{-0.6}$	$17.7^{+1.1}_{-1.8}$	74–88	110–121	147–164	−0.80	−1.40

Note. The $\tilde{\chi}^2$ values are for 3 DOF fits within the 20–60 u q^{-1} range and the superscripts and subscripts correspond to a 2σ deviation. Here, note that for $p = 0.05$ we obtain a critical $\tilde{\chi}^2 = 2.60$. The ELS FWHM for a single distribution function is ∼16.7%, and the spacecraft potentials correspond to the nearest RPWS-LP measurement of this parameter to closest approach.

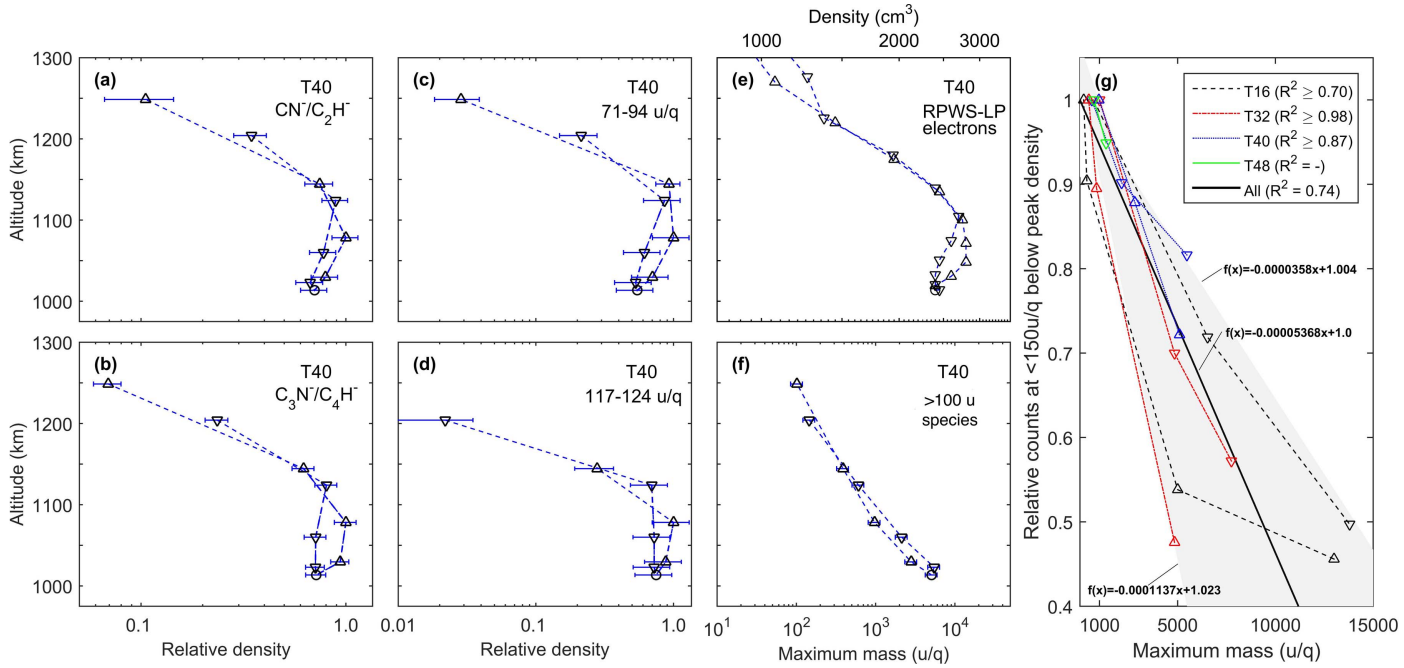

Figure 3. Altitude profiles with ingress (△) and egress (▽) marked. ((a)–(d)) The T40 relative anion densities, (e) the electron density, (f) the maximum mass detected, and (g) the correlation between the depletion of the low-mass (<150 u q^{-1}) anions below the altitude of peak density and corresponding increase in the maximum mass. A linear trend line (black) is fitted as well as individually to the ingress and egress of each encounter, the maximum and minimum of which encompass the region shaded gray. Relative errors are assumed small compared with the overall spread.

phase, whereas the larger $C_{60,70}^{2-}$ molecules can persist for milliseconds (Wang et al. 2009). It therefore appears that multiple charges are much more likely on molecules larger than a few hundred amu in Titan's ionosphere, as indeed was reported by Shebanits et al. (2016).

4. Molecular Growth

Figures 3(a)–(d) show the altitude profiles of peak 1 (25.8–26.0 u q^{-1}, associated with CN^-/C_2H^-), peak 2 (49.0–50.1 u q^{-1}, associated with C_3N^-/C_4H^-), peak 3 (71–94 u q^{-1}), and peak 4 (107–123 u q^{-1}) during the T40 encounter. Figures 3(e)–(f) show the electron densities and maximum detected mass of the larger molecules as obtained in Coates et al. (2009). The altitude profiles in Figure 3 show the carbon chain anions to peak in density above the region where the highest-mass aerosol monomer are observed and to extend several scale heights above this to where the larger species are not present in measurable quantities. While the precise relative densities are not known, the profiles show the negative charge to be increasingly carried by the larger species at lower altitudes. This trend is also observed in further encounters; see Wellbrock et al. (2013) and Figure 3.

Below ∼1100 km the depletion of the <150 u q^{-1} anions can be seen to be related to the size increase of the larger molecules. Figure 3(g) shows this correlation for all encounters except T18, which was omitted as the altitude of peak density of the low-mass ions was not definitively surpassed (indeed, during T48 this was

only surpassed for a brief instance). The two parameters can be seen to be linearly proportional, although there is some spread to the data at the higher masses. This overall proportional decrease in the low-mass species with the increase of the larger species points to dependencies between these.

The data also point to a possible diurnal variation with the dayside measurements grouped together at and above the fitted trend line (black) and the nightside measurements appearing below this and with T16 and T32 crossing Titan's solar terminator. Coates et al. (2009) previously determined significant spatial variations of the high-mass monomers, and these data point to this being echoed in the smaller species. Further statistical analyses are, however, required to fully disentangle such influences.

5. Summary and Conclusions

This study used a forward model of the CAPS-ELS response function to achieve an increased mass resolving capability for anions in Titan ionosphere, the results of which are as follows: the first peak (25.8–26.0 u q^{-1}) and second peak (49.0–50.1 u q^{-1}) in the anion spectrum were statistically shown to be compatible with the CN^-/C_2H^- and C_3N^-/C_4H^-, respectively, although it was not possible to differentiate between these nitrile or hydrocarbon compounds. At altitudes above ~1200 km the third peak is consistent with the further chain anion C_5N^-/C_6H^- but at lower altitudes becomes dominated by higher-mass species not consistent with carbon chain anions. Notably, this is evidence for the presence of more complex structures that may well come to represent the first astrophysical detection of anions not composed of linear chains; see the recent review by Millar et al. (2017). A number of species were suggested to account for this intermediary peak based upon the relatively better understand cation and neutral chemistry. Further persistent detections were also constrained at 117 ± 3 u q^{-1} and 154 ± 6 u q^{-1}, which appear to also add to the growing body of evidence for growth processes involving ring structures, although the current lack of known reaction pathways impedes their definitive interpretation at present.

The evolution of the low-mass (<150 u q^{-1}) anions was then examined with respect to the impending growth of the larger organic molecules. Deep within the ionosphere, the lower-mass anions were observed to become depleted as the larger aerosol precursors coincidentally underwent rapid growth. This trend contributes to the idea that smaller species form the seeds for the larger species via a series of reactions and processes that the chain anions and further intermediary anions appear to be tightly coupled to. These results demonstrate the importance of tracing a route from small to large species in order to fundamentally understand how complex organic molecules can be produced within a planetary atmosphere.

R.T.D. acknowledges STFC Studentship 1429777. A.J.C., A. W., and G.H.J. acknowledge support from the STFC consolidated grants to UCL-MSSL ST/K000977/1 and ST/N000722/1. D.G.C. acknowledges Becas-Chile CONICYT Fellowship (No. 72150555). O.S. acknowledges funding from SNSB, Dnr 130/11:2

References

Ali, A., Sittler, E. C., Chornay, D., Rowe, B. R., & Puzzarini, C. 2015, P&SS, 109, 46
Bettens, R. P. A., & Herbst, E. 1996, ApJ, 468, 686
Broadfoot, A. L., Atreya, S. K., Bertaux, J. L., et al. 1989, Sci, 246, 1459
Coates, A. J., Crary, F. J., Lewis, G. R., et al. 2007, GeoRL, 34, L22103
Coates, A. J., Wellbrock, A., Lewis, G. R., et al. 2009, P&SS, 57, 1866
Coates, A. J., Wellbrock, A., Lewis, G. R., et al. 2010, FaDi, 147, 295
Coletti, C., & Nazzareno, R. 2012, CP, 398, 168
Cordiner, M. A., Buckle, J. V., Wirström, E. S., Olofsson, A. O. H., & Charnley, S. B. 2013, ApJ, 770, 48
Crary, F. J., Magee, B. A., Mandt, K., et al. 2009, P&SS, 57, 1847
Cravens, T. E., Robertson, I. P., Ledvina, S. A., et al. 2008, GeoRL, 35, L03103
Cravens, T. E., Robertson, I. P., Waite, J. H., et al. 2006, GeoRL, 33, L07105
Danielson, R. E., Caldwell, J. J., & Larach, D. R. 1973, Icar, 20, 437
Dobrijevic, M., Loison, J. C., Hickson, K. M., & Gronoff, G. 2016, Icar, 268, 313
Fenzlaff, H.-P., & Illenberger, E. 1984, Int. J. Mass Spectrom., 59, 185
Fraser, G. W. 2002, Int. J. Mass Spectrom., 215, 13
Gladstone, G. R., Stern, S. A., Ennico, K., et al. 2016, Sci, 351, aad8866
Hagstrum, H. D. 1976, in Int. Workshop on Inelastic Ion-Surface Collisions, ed. N. Tolk (Murray Hill, NJ: Bell Laboratories), 1
Hartle, R. E., Sittler, E. C., Neubauer, F. M., et al. 2006, P&SS, 54, 1211
Jones, G. H., Coates, A. J., & Wellbrock, A. 2011, in 2011 AGU Fall Meeting (San Francisco, CA: AGU), abstract SA13A-1887
Lavvas, P., Yelle, R. V., Koskinen, T., et al. 2013, PNAS, 110, 8
Lewis, G. R., André, N., Arridge, C. S., et al. 2008, P&SS, 56, 901
Lindgren, E. B., Stamm, B., Chan, H., et al. 2016, Icar, 291, 245
Michael, M., Tripathi, S. N., Arya, P., et al. 2011, P&SS, 59, 880
Millar, T. J., Herbst, E., & Bettens, R. P. A. 2000, MNRAS, 316, 195
Millar, T. J., Walsh, C., & Field, T. A. 2017, ChRv, 117, 1765
Miller, S. L., & Urey, H. C. 1959, Sci, 130, 245
Niemann, H. B., Atreya, S. K., Bauer, S. J., et al. 2005, Natur, 438, 779
Olah, G. A. 1972, JAChS, 94, 808
Olah, G. A., Mathew, T., Prakesh, G. K., & Rasul, G. 2016, JAChS, 138, 1717
Peko, B. L., & Stephen, T. M. 2010, Nucl. Int. Meth. Phys. Res., 171, 597
Rymer, A. M., Coates, A. J., Svenes, K., et al. 2001, JGR, 106, 30177
Shebanits, O., Wahlund, J.-E., Edberg, N. J. T., et al. 2016, JGRA, 121, 10075
Shebanits, O., Wahlund, J.-E., Mandt, K., et al. 2013, P&SS, 84, 153
Trainer, M. G., Sebree, J. A., Yoon, Y. H., & Tolbert, M. A. 2013, ApJL, 766, L4
Vervack, R. J., Sandel, B. R., & Strobel, D. F. 2004, Icar, 170, 91
Vuitton, V., Lavvas, P., Yelle, R. V., et al. 2009, P&SS, 57, 1558
Vuitton, V., Yelle, R. V., & Cui, J. 2008, JGRE, 113, E05007
Vuitton, V., Yelle, R. V., & Lavvas, P. 2009, RSPTA, 367, 729
Vuitton, V., Yelle, R. V., & McEwan, M. J. 2007, Icar, 191, 722
Wahlund, J.-E., Galand, M., Müller-Wodarg, I., et al. 2009, P&SS, 57, 1857
Waite, J. H., Niemann, H., Yelle, R. V., et al. 2005, Sci, 308, 982
Waite, J. H., Young, D. T., Cravens, T. E., et al. 2007, Sci, 316, 870
Walsh, C., Harada, N., Herbst, E., & Millar, T. J. 2009, ApJ, 700, 752
Wang, X.-B., & Wang, L.-S. 2009, ARPC, 60, 105
Wang, Z., & Biermaum, V. N. 2016, JChPh, 144, 214304
Wang, Z., Cole, A. C., Demarais, N. J., et al. 2015, JAChS, 137, 10700
Wellbrock, A., Coates, A. J., Jones, G. H., Lewis, G. R., & Waite, J. H. 2013, GeoRL, 40, 4481
Westlake, J. H., Waite, J. H., Carrasco, N., Richard, M., & Cravens, T. 2014, JGRA, 119, 5951
Young, D. T., Berthelier, J. J., Blanc, M., et al. 2004, SSRv, 114, 1